ISA Transactions 169 (2026) 436–446

Contents lists available at ScienceDirect

ISA Transactions

journal homepage: www.elsevier.com/locate/isatrans

Research article

FGO-Tuned 2-DOF PI controller for pressure regulation in centrifugal fans driven by induction motors using an experimentally validated model

Cebrail Turkeri [a], Serdar Ekinci [b], Davut Izci [c], Oleh Kiselychnyk [d,*]

[a] Department of Computer Engineering, Batman University, Batman, Türkiye
[b] Department of Computer Engineering, Bitlis Eren University, Bitlis, Türkiye
[c] Department of Electrical-Electronics Engineering, Bursa Uludag University, Bursa, Türkiye
[d] School of Engineering, University of Warwick, Coventry, UK

ARTICLE INFO

Keywords:
Fungal growth optimizer
2-DOF PI controller
Pressure control
Centrifugal fan

ABSTRACT

This study proposes a novel pressure control strategy for a centrifugal fan driven by an induction motor, using a two-degree-of-freedom (2-DOF) proportional-integral (PI) controller optimized via the fungal growth optimizer (FGO). Built upon a validated nonlinear model, the FGO algorithm tunes the controller parameters to minimize a cost function reflecting overshoot and tracking error. Comparative evaluations are performed against genetic algorithm (GA), L-SHADE, and the Newton-Raphson-based optimizer (NRBO), as well as classical methods such as Cohen-Coon and Rovira techniques. The FGO-based controller demonstrates superior dynamic response, robustness, and noise immunity. Statistical validation using the Wilcoxon signed-rank test confirms the performance improvements. These results highlight the effectiveness of FGO in real-world pressure regulation and establish a benchmark for modern industrial fan control systems.

1. Introduction

Centrifugal turbomachinery, comprising fans, pumps, and compressors, are essential components in a wide array of industrial and residential systems. These machines facilitate energy transfer between a rotating shaft and a working fluid, making them vital in processes that demand fluid motion and pressure regulation [1,2]. In industrial settings, centrifugal compressors are widely used for gas processing, oil refineries, and chemical plants, while centrifugal pumps serve in water supply systems, cooling circuits, and irrigation infrastructure [3–6]. In residential and commercial applications, centrifugal fans are foundational elements in heating, ventilation, and air conditioning (HVAC) systems, where they ensure proper air circulation and temperature control [7,8]. Their ubiquity and critical function underscore the necessity of ensuring reliable and efficient performance, particularly through accurate pressure control strategies [9].

Effective pressure regulation in centrifugal turbomachines plays a vital role in maintaining operational safety, energy efficiency, and overall system stability. Whether in compressors, pumps, or fans, precise control of pressure is essential to avoid instabilities such as surge, to ensure consistent flow delivery and to achieve optimal energy use [10]. Given the broad applicability of these machines, pressure control remains an area of significant research and engineering focus.

A wide range of advanced control methods have been proposed for pressure regulation in turbomachinery. Notably, model predictive control (MPC) and H-infinity control have been adopted for their robustness and ability to handle multi-variable and constrained systems [11,12]. Paper [13] applied nonlinear optimal H-infinity control to compressor systems, while [14] emphasized the MPC approaches for active surge control in centrifugal compressors. Moreover, predictive strategies integrated with machine learning approaches such as Gaussian process regression (GPR) have further improved adaptability and tracking performance [15]. In parallel with these developments, there has also been growing interest in sensorless control techniques. These methods eliminate the need for physical pressure sensors, instead estimating pressure via software-based approaches such as the extended Kalman filter (EKF) or artificial neural networks (ANN) [16,17]. Similarly, [18] presented experimentally validated dynamic models and ANN-based estimators for pressure and flow rate in centrifugal fans driven by induction motors, forming a foundation that supports advanced control as well as data-driven tuning.

Despite the effectiveness of advanced controllers, their

* Corresponding author.
E-mail addresses: cebrail.turkeri@batman.edu.tr (C. Turkeri), sekinci@beu.edu.tr (S. Ekinci), davutizci@uludag.edu.tr (D. Izci), O.Kiselychnyk@warwick.ac.uk (O. Kiselychnyk).

https://doi.org/10.1016/j.isatra.2025.12.012
Received 7 July 2025; Received in revised form 5 December 2025; Accepted 5 December 2025
Available online 10 December 2025
0019-0578/© 2025 The Authors. Published by Elsevier Ltd on behalf of International Society of Automation. This is an open access article under the CC BY license (http://creativecommons.org/licenses/by/4.0/).

implementation complexity, high computational demands, and reliance on precise system modeling often limit their practical adoption in industrial environments. As a result, traditional control methods such as Proportional-Integral (PI) [19,20] and Proportional-Integral-Derivative (PID) controllers [21,22] remain dominant in industry due to their structural simplicity and satisfactory performance for a wide range of operating conditions. These controllers are often sufficient for applications where modeling uncertainties and dynamic variations are moderate.

Nevertheless, the key challenge with PI and PID controllers lies in tuning their parameters appropriately. In practice, a variety of tuning methods are employed to optimize their behavior. Among the most commonly used are empirical methods such as Ziegler-Nichols [23], Cohen-Coon [24], and Rovira [25]. These methods provide quick initial settings but tend to offer suboptimal performance in nonlinear, time-varying, or load-dependent scenarios [26,27]. Moreover, the limited adaptability of these tuning rules becomes more apparent as control systems encounter complex operational regimes.

To overcome the limitations of classical tuning approaches, heuristic and metaheuristic optimization methods have gained considerable attention in recent years. These methods use nature-inspired algorithms to explore a broader search space and find globally optimal or near-optimal controller settings [28]. Algorithms such as genetic algorithm (GA) [29], particle swarm optimization (PSO) [30], ant colony optimization (ACO) [31], simulated annealing (SA) [32], and electric eel foraging optimizer (EEFO) [33] have been widely applied for PID tuning. Bekhiti and Nail [34] employed the grey wolf optimizer (GWO) for pressure-temperature control in centrifugal compressors and reported significant improvements in transient response. Additionally, more recent strategies such as sine cosine algorithm (SCA) [35] and Newton Raphson based optimizer (NRBO) [36] methods have shown promising results in nonlinear control systems. Other notable developments include the use of cuckoo search [37] and whale optimization algorithm (WOA) [38]. Furthermore, L-SHADE, introduced by Tanabe and Fukunaga, has been recognized as a leading algorithm in CEC competitions due to its robust convergence and adaptability [39]. Among the newest entries in the field is the fungal growth optimizer (FGO), introduced by Abdel-Basset et al. [40]. FGO introduces a hybrid strategy combining chemotropism-based directed search and stochastic branching mechanisms [40]. These properties allow FGO to avoid premature convergence and enhance global search capabilities, which are particularly beneficial in highly nonlinear and multidimensional control parameter optimization problems. Moreover, FGO has shown competitive performance in recent benchmark studies and has not yet been applied in the context of pressure control systems or 2-DOF PI controller tuning, thus providing both theoretical and application-level novelty.

In parallel with the development of optimization techniques, attention has shifted to control structures that offer better separation between setpoint tracking and disturbance rejection. The two-degree-of-freedom (2-DOF) PI controller has emerged as a strong candidate in this regard. Unlike conventional PI and PID controllers, which rely on a single feedback loop, the 2-DOF structure introduces a reference weighting factor a that allows for more flexible tuning of transient response without compromising robustness [41].

However, despite their practical benefits, their application to nonlinear pressure control of centrifugal fans driven by induction motors remains largely unexplored in the literature. This motivates the present study, which employs FGO to tune a 2-DOF PI controller, building upon the experimentally validated dynamical model in [18]. Benefiting from its ability to decouple setpoint tracking from disturbance rejection and to flexibly adjust transient performance via the reference weighting factor α without compromising robustness, the 2-DOF PI controller offers a compelling solution for this industrial application. This combination aims to enhance the tracking performance, robustness, and stability of pressure control in centrifugal fans. The proposed methodology not only compares the FGO-based controller with classical tuning methods such as Cohen-Coon and Rovira [24,25], which are widely known empirical rules, but also benchmarks its performance against representative metaheuristic techniques. Specifically, NRBO [36] is included as one of the most recent algorithms in the literature, L-SHADE [39] is selected due to its superior performance in benchmark competitions such as the IEEE CEC, and GA [29] is chosen for being one of the earliest and most widely used evolutionary optimization methods. This selection ensures that the proposed approach is evaluated against state-of-the-art, historically significant, and practically common tuning strategies.

Unlike previous studies, which applied 2-DOF PI/PID controllers in unrelated domains or tuned them using other approaches, the present work uniquely combines the FGO-based tuning with a 2-DOF PI controller for centrifugal fan pressure control, implemented on a previously validated nonlinear fan-motor model. The study also delivers a comprehensive performance evaluation, including robustness, noise immunity, and disturbance rejection, within this industrial application.

The main features and evaluation framework of this study are as follows:

- A novel application of the FGO algorithm is introduced to tune a 2-DOF PI controller for pressure regulation in centrifugal fans.
- A previously validated nonlinear dynamical model of a fan-induction motor system is employed as the plant model, onto which the proposed FGO-optimized 2-DOF-PI controller is implemented for the first time.
- Comparative analysis includes: Cohen-Coon, Rovira (traditional tuning methods), GA (widely used), L-SHADE (CEC benchmark winner), and NRBO (recent state-of-the-art algorithm).
- The evaluation metrics comprise; boxplot visualization of multiple runs, convergence analysis of cost functions, Wilcoxon signed-rank test for statistical validation, time-domain tracking under diverse conditions, disturbance rejection and noise attenuation performance.

The remainder of this paper is organized as follows: Section 2 details the mathematical modeling of the pressure control system. Section 3 introduces the FGO algorithm. Section 4 outlines the controller design and optimization procedure. Section 5 presents comparative performance analysis. Finally, Section 6 concludes the study.

2. Dynamical model of the centrifugal fan driven by a three-phase induction motor

In this study, the nonlinear dynamical model of the centrifugal fan driven by a three-phase squirrel-cage induction motor is adopted from [18], which has been experimentally validated. This model forms the foundational framework for the controller development and simulation-based performance evaluation, providing high credibility for the validation of the proposed control strategy.

The airflow dynamics within the fan housing are governed by the following differential equation:

$$\chi \frac{dQ}{dt} = H_{or}\left(\frac{\omega}{\omega_r}\right)^2 - a_f Q^2 - b_f Q - a_n Q^2 \tag{1}$$

where Q is the flow rate, ω is the angular velocity of the fan and ω_r is the rated angular velocity. H_{or} denotes the pressure at zero flow rate and rated velocity, The coefficients a_f and b_f are approximation parameters for modeling the fan's nonlinear Q-H (flow-pressure) characteristic at rated speed, while a_n is used to approximate the duct air resistance. The parameter χ is an integration constant that governs the inertial dynamics of the airflow in the fan housing. The internal fan pressure is modeled using the first three terms of the right-hand side of Eq. (1):

$$H = H_{or}\left(\frac{\omega}{\omega_r}\right)^2 - a_f Q^2 - b_f Q \tag{2}$$

The overall efficiency of the fan-motor system is defined as the ratio of output power to the motor's active input power:

$$\eta_c = \frac{P_{out}}{P_{input}} = \frac{QH}{P_{input}} \tag{3}$$

To increase modelling accuracy, a neural network estimator is employed to evaluate the combined system efficiency η_c based on experimental input-output data. The estimator uses three inputs: flow rate Q, pressure H and motor voltage frequency $f$such that:

$$\eta_c = f(Q,H,f) \tag{4}$$

The fan's own efficiency η_f is computed as a ratio between the overall system efficiency η_c and the motor efficiency η_m:

$$\eta_f = \frac{\eta_c}{\eta_m} \tag{5}$$

The motor's efficiency η_m is computed using developed motor's shaft power (the product of torque T and angular velocity ω) and power loss P_{loss}:

$$\eta_m = \frac{T\omega}{T\omega + P_{loss}} \tag{6}$$

where P_{loss} includes only copper losses. The mechanical loss and loss due to magnetic effects (iron loss) are attributed to the fan/pump for simplicity, via the combined efficiency.

The load torque developed by the fan at the motor shaft is obtained via:

$$T_L = \frac{P_{out}}{\eta_f \omega} = \frac{QH\eta_m}{\omega \eta_c(Q,H,f)} \tag{7}$$

This expression links the mechanical load torque to the dynamic states and efficiency estimates, enabling accurate representation of the interaction between fan and motor.

The induction motor itself is modelled using a standard five-equation representation in the α–β stationary reference frame, assuming scalar open-loop speed control. Although the detailed differential equations are omitted here for brevity, they follow the established modelling framework for three-phase induction machines and can be implemented via the *Asynchronous Machine SI Units* block in MATLAB/Simulink/Simscape. The angular velocity is the output of the motor model. The inputs are three-phase sinusoidal voltages with a reference frequency and a reference amplitude, and the motor load torque. The V/f^2=const relationship between the reference frequency and the reference amplitude is set externally, including saturation at rated values. The model also computes both stator and rotor currents allowing to determine the motor copper loss. By integrating the nonlinear fan model and the validated motor model (via the velocity and load torque), the complete system serves as a high-fidelity simulation platform. Since this model has been experimentally validated, the control designs applied in this study are directly implemented and tested on a reliable simulation basis, ensuring practical credibility and accuracy.

3. FGO

FGO is a recent metaheuristic algorithm inspired by the adaptive behaviors of fungi in nature, particularly hyphal tip extension, chemotropic movement, and branching mechanisms. These behaviors allow fungi to explore and exploit their environment efficiently, making FGO a powerful framework for solving complex, nonlinear optimization problems [40].

FGO starts by initializing a population of agents called hyphae, each representing a candidate solution. The initial positions of these hyphae are randomly generated across the defined search space $\boldsymbol{S} \in \mathbb{R}^d$ using:

$$\vec{S}_i^{\,0} = \vec{S}_L + r \odot \left(\vec{S}_U - \vec{S}_L\right), \mathrm{i} = 1, \quad 2, \quad \ldots, \mathrm{N} \tag{8}$$

where i denotes the index of the hypha in the population, where i $= 1,$ 2, ….,N, $\vec{S}_L$ and $\vec{S}_U$ are the lower and upper bounds of the search space, $\odot$ denotes element-wise multiplication (Hadamard product) and $r \in [0,1]^d$ is a uniformly distributed random vector. Each hypha then undergoes an iterative growth process. At each iteration t, a hypha may either continue growth along its tip, branch laterally, or initiate a new germination depending on its relative performance and a set of stochastic rules. The updated dynamics are governed by a balance between two main behaviors: exploration and exploitation.

3.1. Hyphal tip growth and exploration

Exploration in FGO is modeled through directional extension of hyphae toward diverse regions of the search space. The extension is driven by a growth rate E computed as:

$$E = \exp\left(\frac{f_i}{\sum_{j=1}^{N} f_j}\right) \times r_1 \times \left(1 - \frac{t}{t_{\max}}\right)^{\left(1 - \frac{t}{t_{\max}}\right)} \tag{9}$$

where f_i denotes the fitness of the i-th solution, r_1 is a uniformly distributed random number in $[0,1]$ and $t_{\max}$ is the maximum number of iterations. The new direction $\vec{D}$ is defined by the difference between two randomly selected solution vectors:

$$\vec{D} = \vec{S}_a^{\,t} - \vec{S}_b^{\,t} \tag{10}$$

where a and b are the indexes of two distinct randomly selected hyphae from the population at iteration t. Then, the position is updated as:

$$\vec{S}_i^{\,t+1} = \vec{S}_i^{\,t} + E \times \vec{D} \tag{11}$$

To enhance exploration selectively in dimensions, a probabilistic filtering mechanism updates only certain components of the position vector:

$$\vec{S}_{ij}^{\,t+1} = \begin{cases} \vec{S}_{ij}^{\,t+1}, \textit{if } R_j > r_3 \\ \vec{S}_{ij}^{\,t}, \textit{otherwise} \end{cases} \textit{for } j = 1, \ldots, \quad d \tag{12}$$

where $R_j \sim \mathscr{U}(0,1)$ is the random number for the j^{th} dimension and $r_3 \in [0,1]$ is a threshold value.

3.2. Chemotropism-based exploitation

In the FGO algorithm, exploitation is modeled based on the chemotropism behavior of fungal hyphae, which enables directional growth toward favorable nutrient sources. This is mathematically expressed as:

$$\vec{D}_i^{\,e} = r_4 \times \left(\vec{S}_a^{\,t} - \vec{S}_i^{\,t}\right) + r_5 \odot \left(\beta \times \vec{S}^{\,*} - \vec{S}_i^{\,t}\right)[r_6 > R] \tag{13}$$

where $\vec{S}_i^{\,t}$ is the current solution (hypha), $\vec{S}_a^{\,t}$ is a randomly selected solution from the population, $\vec{S}^{\,*}$ is the global best solution found so far, r_4, r_5, $r_6 \in [0,1]$ are random values generated from a uniform distribution, $\beta \in \{-1,+1\}$, is a direction control coefficient randomly chosen, $R \in [0,1]$ is a predefined threshold constant and $[r_6 > R]$ is an Iverson bracket, which evaluates to:

$$[r_6 > R] = \begin{cases} 1, \textit{ if } r_6 > R \\ 0, \textit{ otherwise} \end{cases} \tag{14}$$

This operator balances random directional movement (first term) with greedy attraction to the global best (second term), but the latter is only activated when $r_6 > R$, providing conditional exploitation that enhances adaptability and avoids premature convergence. To adjust the

aggressiveness of exploitation, an adaptive step size η_i is defined as:

$$\eta_i = \begin{cases} r_7, \ if\ t < \dfrac{t_{\max}}{2} \\ \dfrac{\eta_i}{\sum_{k=1}^{N}\eta_k} + 2r_8, \ otherwise \end{cases}, \ i = 1,\ 2,\quad \ldots,\quad N \tag{15}$$

where r_7 and r_8 are random numbers between 0 and 1. The position update rule incorporates both directional movement and a local perturbation vector $\overrightarrow{E}_c$:

$$\begin{gathered} \overrightarrow{S}_i^{t+1} = \overrightarrow{S}_i^{t} + \eta_i \times \overrightarrow{D}_i^{e} + \overrightarrow{E}_c \times \left[r_{12} > E_p\right] \\ \overrightarrow{E}_c = (r_9 - 0.5) \times r_{10} \odot \left(\overrightarrow{S}_a^{t} - \overrightarrow{S}_b^{t}\right) \end{gathered}, \ \left[r_{12} > E_p\right] = \begin{cases} 1, \ if\ r_{12} > E_p \\ 0, \ otherwise \end{cases} \tag{16}$$

where $E_p \in [0,1]$ is a fixed perturbation probability threshold and r_{12} is a random number. $\overrightarrow{S}_a^{t}$ and $\overrightarrow{S}_b^{t}$ are two distinct solutions. A greedy selection strategy is adopted:

$$\overrightarrow{S}_i^{t+1} = \begin{cases} \overrightarrow{S}_i^{t} + \eta_i \times \overrightarrow{D}_i^{e2} + \overrightarrow{E}_c \times [r_{11} > r_{13}],\ r_{14} < r_{15} \\ \overrightarrow{S}_i^{t} + \eta_i \times \overrightarrow{D}_i^{e} + \overrightarrow{E}_c \times \left[r_{12} > E_p\right],\ else \end{cases}, \ i = 1,\ 2,\ \ldots,\ N \tag{17}$$

where r_9, r_{10}, r_{11}, r_{12}, r_{13}, r_{14}, $r_{15} \in [0,1]$ are random scaling factors.

To balance exploration and exploitation adaptively, each individual is assigned an exploration probability:

$$p_i = \frac{f_i - f_{\min}}{f_{\max} - f_{\min} + \varepsilon} \tag{18}$$

where $f_{\min}$ and $f_{\max}$ denote the best and worst fitness values in the current population, ε is a small constant to avoid division by zero. An adaptive factor controlling exploration pressure is defined as:

$$E_r = \mathscr{M} + (1 + \mathscr{M}) \times \left(1 - \frac{t}{t_{\max}}\right) \tag{19}$$

where $\mathscr{M} \in [0,1]$ is a constant controlling minimum exploitation pressure.

3.3. Hyphal branching and spore germination

In the later stage of fungal evolution, when the growth of a hypha becomes unstable or encounters stressors such as nutrient deficiency or external environmental perturbations, the hypha may branch or germinate spores to enhance exploration and adaptation. FGO models this behavior through a set of equations that enable both lateral branching and spore-based diversification.

To begin with, two directional growth patterns are considered for generating new hyphae. The first pattern is based on the difference between two randomly selected individuals from the population:

$$\begin{aligned} \overrightarrow{D}_i^{ep1} &= \left(\overrightarrow{S}_a^{t} - \overrightarrow{S}_b^{t}\right) \\ \overrightarrow{D}_i^{ep2} &= \left(\overrightarrow{S}_c^{t} - \overrightarrow{S}^{*}\right) \end{aligned} \tag{20}$$

The direction of the new hypha is then determined by combining these two patterns based on a uniformly distributed random number r_5.

$$\overrightarrow{S}_i^{t+1} = \overrightarrow{S}_i^{t} + r_5 \times \overrightarrow{D}_i^{ep1} + (1 - r_5) \times \overrightarrow{D}_i^{ep2} \tag{21}$$

To account for growth dynamics under varying environmental conditions, the lateral growth rate is defined as follows:

$$E^L = 1 + e^{\frac{f_i}{\sum_{k=1}^{N} f_k}} \times [r_6 < r_7] \tag{22}$$

where f_k denotes the fitness value of the k-th individual. The Iverson bracket $[r_6 < r_7]$ equals 1 if the condition is true, and 0 otherwise. Using this dynamic growth rate, the updated lateral branching position for each dimension $j = 1,\ 2, \ldots, d$ is formulated as:

$$\begin{aligned} S_i^{t+1} = \left[R_j < r_3\right] \times S_{i,j}^{t} + \big(1 - \left[R_j \right. \\ \left. < r_3\right]\big) \times \left(S_{i,j}^{t} + r_5 \times E^L \times D_i^{ep1} + (1 - r_5) \times E^L \times D_i^{ep2}\right) \end{aligned} \tag{23}$$

where $R_j \in [0,1]$ is a uniformly distributed random value for the j-th dimension. The model also introduces a spore germination mechanism to increase solution diversity. A new hypha is generated using the absolute difference between the mean of three randomly selected individuals and the current solution. Let $S_{a,j}^{t}$, $S_{b,j}^{t}$, $S_{c,j}^{t}$ denote randomly chosen individuals, then the spore germination update rule is given by:

$$\begin{aligned} S_{i,j}^{t+1} = \left[R_j < r_3\right] \times S_{i,j}^{t} + \left(1 - \left[R_j < r_3\right]\right) \times \\ \left(\frac{\left(\left(\frac{t}{t_{\max}}\right) \times S_j^{*} + \left(1 - \frac{t}{t_{\max}}\right) \times S_{a,j}^{t} \right)}{2} + \overrightarrow{S}_b^{t} \right) \\ \overline{\qquad\qquad 2 \qquad\qquad} + S_g r_5 E \times \left| \frac{S_{a,j}^{t} + S_{b,j}^{t} + S_{c,j}^{t}}{3} - S_{i,j}^{t} \right| \end{aligned} \tag{24}$$

Here, $S_g \in \{-1, +1\}$ is a randomly selected sign that dictates the direction of spore movement, and E is the exponential growth rate parameter.

Finally, the trade-off between branching and spore germination is determined stochastically. With a 50 % probability, one of the two perturbation strategies is applied:

$$\overrightarrow{S}_i^{t+1} = \begin{cases} Apply\ Eq.\ (23)\ r_7 < 0.5 \\ Apply\ Eq.\ (24),\ else \end{cases} \tag{25}$$

These equations collectively model the branching and reproduction capabilities of fungal hyphae within the FGO framework, ensuring both local exploitation and global exploration for optimal solution discovery.

The full optimization procedure of the proposed FGO algorithm, integrating exploration, exploitation, lateral branching, and spore germination mechanisms, is summarized in the flowchart provided in Fig. 1.

4. A Novel control strategy for pressure control of centrifugal fan

To ensure effective pressure regulation in centrifugal

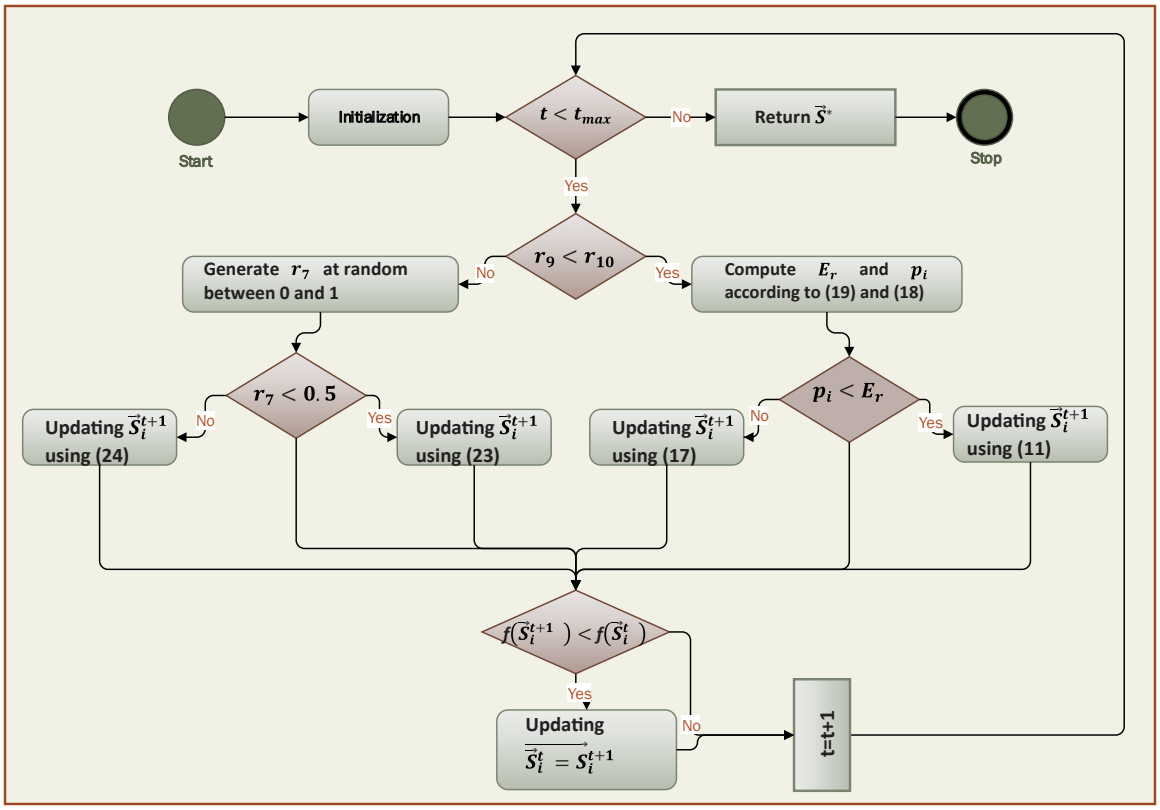


Fig. 1. Working mechanism of FGO.

turbomachinery, a novel control strategy is developed based on the two-degree-of-freedom (2-DOF) proportional-integral (PI) controller architecture. The control objective is to maintain the desired pressure level despite nonlinearities, disturbances, and system uncertainties inherent in the fan-motor system.

To regulate the system output, the control signal input $U(s)$ is generated using the 2-DOF PI controller showed in Eq. (26). In this configuration, the control signal (frequency) is applied to the 3-phase induction motor, which in turn drives the centrifugal fan to regulate the output pressure based on the reference setpoint. Although PID controllers are widely used in industrial systems, this study deliberately adopted a 2-DOF PI structure without a derivative component for the following reason. The 2-DOF architecture inherently enables decoupling of setpoint tracking and disturbance rejection through the reference-weighting factor α, which allows tuning of transient response separately from robustness requirements [42]. This capability partially compensates for the damping effect typically introduced by the D term, enabling comparable performance without its noise amplification drawbacks.

$$U(s) = K_p[\alpha R(s) - Y(s)] + \frac{K_i}{s}[R(s) - Y(s)] \tag{26}$$

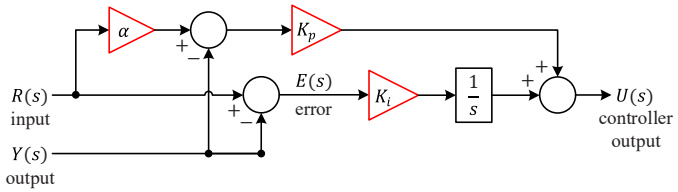


Fig. 2. Block diagram of 2-DOF PI controller.

where $R(s)$ is the reference (setpoint), $Y(s)$ is the output (measured fan pressure), K_p and K_i are the proportional and integral gains, respectively and α is the setpoint weighting factor, which enables decoupling of reference tracking from feedback regulation, thereby allowing additional tuning flexibility over the reference input dynamics [42]. This feature enhances the transient response performance, particularly overshoot and rise time, without affecting disturbance rejection. The corresponding block diagram representation of this controller is illustrated in Fig. 2.

To implement this control strategy, the 2-DOF PI controller was embedded into the closed-loop system consisting of the induction motor and centrifugal fan, as shown in Fig. 3.

The optimal values of the controller parameters K_p, K_i and α were obtained using the FGO algorithm by minimizing a composite cost function CF, which evaluates control performance in terms of overshoot and tracking accuracy. The cost function is defined as:

$$CF = (1-\varphi)\cdot OS + \varphi \int_0^{t_f} |e(t)|dt \tag{27}$$

where $\varphi = 0.8$ is the weight factor, selected based on preliminary sensitivity analyses to balance the relative importance of overshoot minimization and transient tracking performance. Lower φ values overly prioritize overshoot suppression at the expense of reference tracking speed, while higher φ values enhance transient responsiveness but permit excessive overshoot. The choice of 0.8 was found to provide a well-balanced trade-off between these two objectives in the studied system. OS is the normalized percent overshoot, $e(t) = r(t) - y(t)$ is the instantaneous control error, and $t_f = 30$ s is the simulation horizon. In addition, the search space for the FGO optimization was bounded as $0.001 \le K_p \le 0.3$, $0.001 \le K_i \le 0.3$, and $0.8 \le \alpha \le 1.2$. These limits

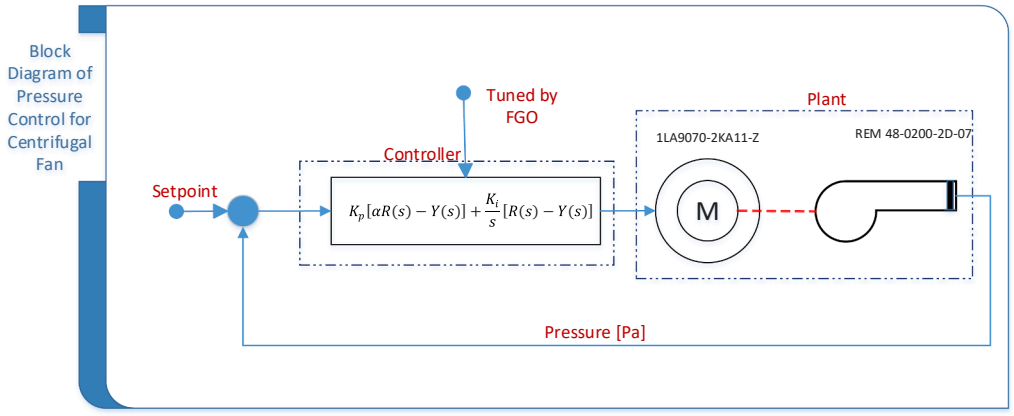


Fig. 3. Closed-loop implementation of the pressure control system using an FGO-tuned 2-DOF PI controller.

were determined through an extensive trial-and-error process combined with preliminary stability and performance analysis on the present nonlinear fan–motor model. The lower bounds were set to avoid excessively sluggish responses, while the upper bounds were chosen to prevent instability and actuator saturation. The selected α range provides sufficient flexibility for shaping the transient response without leading to overshoot-dominated behavior.

During optimization, each candidate solution in the FGO population encodes a triplet $[K_p, K_i, \alpha]$ within the specified bounds. For every candidate, the closed-loop nonlinear fan-motor system is simulated under a step change in the reference signal. The objective function, combining *OS* and the integral of the absolute error (IAE), is computed to assess performance. The FGO algorithm then updates the candidate set iteratively using its exploration and exploitation dynamics, progressively guiding the search toward parameter combinations that minimize the objective. The optimal controller gains are taken from the best-performing candidate upon meeting the termination criterion.

The overall control structure including the controller, motor, and fan is shown in Fig. 3, where the system operates in a closed loop to maintain the desired pressure output. The REM 48–0200–2D-07 is an industrial centrifugal fan from Nicotra-Gebhardt, while the 1LA9070–2KA11-Z is a 0.37 kW squirrel-cage induction motor from Siemens, used in the previously validated experimental system [18].

5. Comparative simulation results

To rigorously evaluate the effectiveness of the proposed 2-DOF PI controller optimized via the FGO, comparative simulations using the system parameters from [18] were conducted against three well-established optimization algorithms: GA, L-SHADE, and NRBO. These algorithms were chosen based on their relevance and prominence in the literature. Specifically, GA is among the most widely used evolutionary algorithms, known for its versatility and ease of implementation. L-SHADE is a highly competitive differential evolution variant, having consistently demonstrated superior performance in CEC competitions. NRBO, on the other hand, represents a recently proposed metaheuristic, designed to achieve better exploitation-exploration balance through novel movement operators. This selection allows for a comprehensive comparison of the proposed FGO method with classical, competitive, and state-of-the-art approaches.

All algorithms were executed under identical simulation conditions to ensure fairness: 25 independent runs, a population size of 30, and a maximum iteration count of 100. The reference pressure is 745 Pa, corresponding to the optimal operating point of the centrifugal fan, as determined experimentally [18].

Fig. 4 shows the cost function values achieved over the 25 runs for each algorithm. Among them, the FGO consistently produces lower cost values, as indicated by the blue curve, which lies below the others in the majority of runs. L-SHADE (yellow), NRBO (orange), and particularly

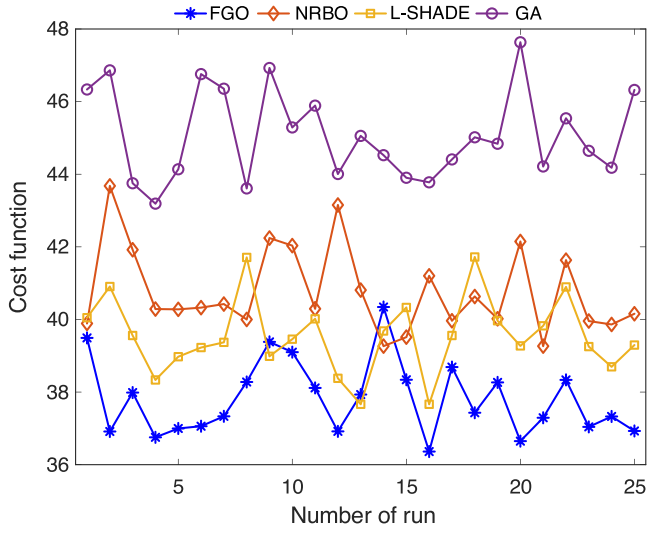


Fig. 4. Cost function values achieved over the 25 runs.

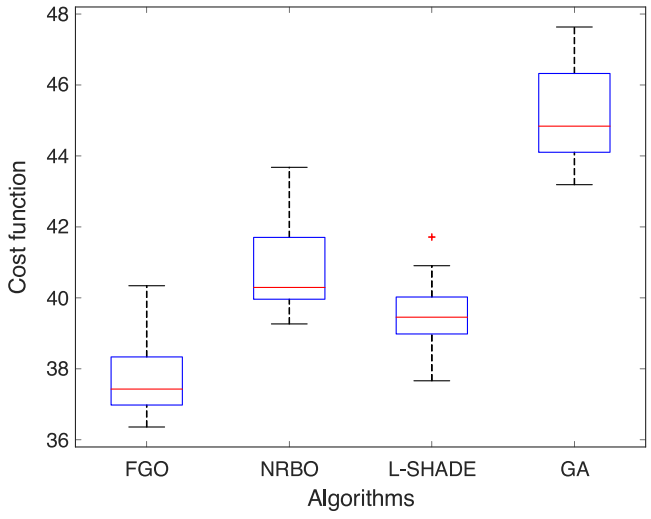


Fig. 5. Boxplot analysis of FGO, NRBO, L-SHADE and GA.

Table 1
Numerical statistical performance metrics.

Algorithm	Average	SD	Best	Worst	Median
FGO	37.8106	1.0186	36.3614	40.3430	37.4304
NRBO	40.7583	1.1839	39.2657	43.6792	40.2945
L-SHADE	39.5516	1.0425	37.6639	41.7203	39.4567
GA	45.0869	1.2378	43.1903	47.6346	44.8402

GA (purple) yield comparatively higher costs, revealing FGO's consistent superiority in convergence reliability and performance.

To provide a statistical overview, Fig. 5 presents a boxplot analysis for all algorithms. FGO exhibits the lowest median cost and tightest interquartile range, indicating not only optimal performance but also high robustness and low variability. The presence of an outlier in L-SHADE, denoted by the plus symbol above the box, suggests occasional instability in its convergence. Meanwhile, GA demonstrates the widest spread and highest cost values, further validating the strength of the proposed FGO-based strategy.

Numerical statistical performance metrics are tabulated in Table 1, which includes average, standard deviation (SD), best, worst, and median cost values. It is evident that FGO surpasses all competitors across every criterion, achieving the best performance with the lowest variability.

To statistically verify these observations, the Wilcoxon signed-rank test was employed. The results, summarized in Table 2, confirm that the performance difference between FGO and the other algorithms is statistically significant, with all p-values far below 0.05, establishing FGO as the consistent winner in every pairwise comparison.

Table 2
Wilcoxon signed-rank test.

FGO versus NRBO		FGO versus L-SHADE		FGO versus GA	
p-value	Winner	p-value	Winner	p-value	Winner
1.5705E−05	FGO	3.6243E−05	FGO	1.2290E−05	FGO

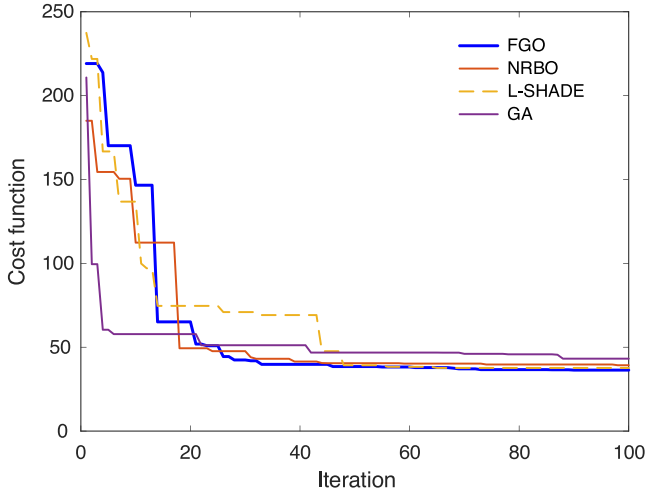


Fig. 6. Evolution of *CF* cost function.

Table 3
Optimal 2-DOF PI controller parameters determined by different optimization algorithms.

Algorithm	K_p	K_i	α
FGO	0.29493	0.20396	1.04898
NRBO	0.26320	0.09314	1.07933
L-SHADE	0.27954	0.15437	1.06148
GA	0.24319	0.16276	1.06213

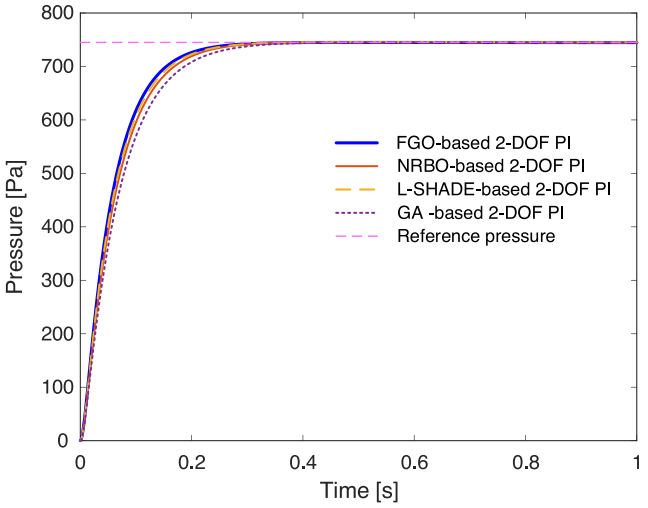


Fig. 7. Time response of FGO based 2-DOF PI against NRBO, L-SHADE and GA.

Table 4
Comparisons of normalized time response specifications.

Control mechanism	Rise time (s)	Settling time (s)	Overshoot (%)	Steady-state error (%)
FGO-based 2-DOF PI	**0.1172**	**0.2120**	**0**	**1.1993E−09**
NRBO-based 2-DOF PI	0.1285	0.2299	0.1118	4.9882E−06
L-SHADE-based 2-DOF PI	0.1226	0.2205	0.0516	4.3554E−08
GA-based 2-DOF PI	0.1426	0.2564	0.0223	2.8576E−09

Fig. 6 illustrates the evolution of the CF cost function over 100 iterations. Although GA initially decreases more rapidly, it stagnates at higher cost levels, while FGO continues a steady descent and ultimately converges to the lowest final cost, highlighting its effectiveness in fine-tuning controller parameters. The convergence curves in Fig. 6 and the controller parameters listed in Table 3 correspond to the best-performing trial among 25 independent runs for each algorithm (16th run for FGO, 14th for NRBO, 13th for L-SHADE, and 4th for GA).

Table 3 provides the final values of K_p, K_i and α obtained from each optimization algorithm. While these parameter values vary across

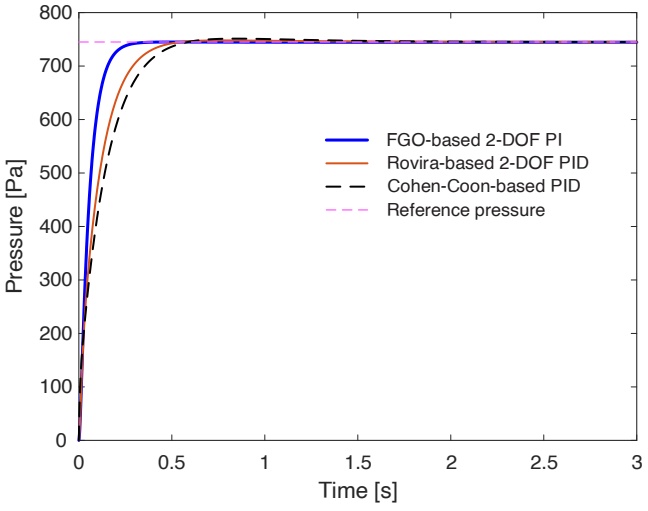


Fig. 8. Time response of FGO based 2-DOF PI against Rovira based 2-DOF PID and Cohen-Coon based PID methods.

methods, it is the resulting control performance, as reflected in the cost function, that serves as the primary measure of effectiveness. FGO-tuned gains lie within the predefined bounds and contribute directly to its superior results.

Fig. 7 involves the step time response of pressure output controlled by four different optimization-based 2-DOF PI controllers. These are the FGO, NRBO, L-SHADE, and GA tuned controllers. All controllers attempt to track the same reference pressure. Among them, the FGO-based controller demonstrates the most rapid and smooth rise, reaching the reference pressure with minimal deviation and without introducing overshoot, whereas the GA-based controller exhibits a slightly slower response with noticeable lag during the rise phase.

To quantitatively validate the performance differences observed in Fig. 7, the normalized time-domain specifications are summarized in Table 4. The rise time is computed between 10 % and 90 % of the final value, while the normalized settling time is defined using a $\pm$ 2 % tolerance band. The steady-state error is calculated at the final simulation time $t_f = 30\ s$. As observed, the FGO-based 2-DOF PI controller significantly outperforms the alternatives, achieving the fastest rise time of 0.1172 s and the shortest settling time of 0.2120 s. Moreover, the FGO controller completely eliminates overshoot, confirming its superior dynamic performance.

Further validation is presented in Fig. 8, where the FGO-based 2-DOF PI controller is benchmarked against two classical tuning methods: Rovira-based 2-DOF PID and the Cohen-Coon-based PID controllers. The step response clearly shows that the FGO-based design yields a more agile response with a faster rise and no overshoot, while both classical methods demonstrate slower convergence and higher transient deviations. For completeness, the controller parameters are as follows: Parameters of Rovira-based 2-DOF PID controller are $K_p = 0.17657$, $K_i = 0.23185$, $K_d = 0.00238$, $N = 83.61550$, $\alpha = 1.02598$ and $\beta = 0.96051$. Parameters of Cohen-Coon-based PID controller are $K_p = 0.14739$, $K_i = 0.23953$ and $K_d = 0.00326$.

The corresponding normalized performance metrics are provided in Table 5 to complement the step responses illustrated in Fig. 8. Both classical methods exhibit inferior performance when compared to the FGO-based design. The Rovira-based controller shows moderate overshoot (0.4066 %) and slower dynamics, while the Cohen-Coon-based controller performs even less favorably, with the highest overshoot (0.8442 %) and the longest rise and settling times among the three. These outcomes confirm that traditional tuning methods are less effective in managing the dynamic complexity of the nonlinear system, further highlighting the advantages of optimization-driven control design.

Following the comparative evaluation against the recent, classical and popular metaheuristic tuning methods, the robustness of the proposed FGO-based controller is assessed under varying operational conditions with $r(t)$ defined in Eq. (28) as the input signal. Fig. 9 illustrates the pressure tracking performance of the FGO-based 2-DOF PI controller when subjected to a piecewise constant reference signal. The controller successfully tracks each step change without significant deviation, demonstrating its strong capability in handling multi-operating-point scenarios with consistency and stability.

$$r(t) = \begin{cases} 745\ [Pa] & \text{if } 0s < t \leq 5s \\ 665\ [Pa] & \text{if } 5s < t \leq 10s \\ 770\ [Pa] & \text{if } 10s < t \leq 15s \\ 680\ [Pa] & \text{if } 15s < t \leq 20s \\ 745\ [Pa] & \text{if } 20s < t \leq 25s \end{cases} \tag{28}$$

$$d(t) = \begin{cases} 0\ [Pa] & \text{if } 0s < t \leq 5s \\ 75\ [Pa] & \text{if } 5s < t \leq 10s \\ -60\ [Pa] & \text{if } 10s < t \leq 15s \\ 0\ [Pa] & \text{if } 15s < t \leq 20s \end{cases} \tag{29}$$

Robustness against external disturbances and sensor noise is further examined. Fig. 10 shows the external disturbance and measurement noise profiles that are deliberately injected into the system to evaluate disturbance rejection and noise attenuation capabilities. The disturbance signal $d(t)$ is defined in Eq. (29) and the measurement noise is modeled as band-limited white noise with a noise power of 0.05 W and a sample time of 0.02 s. To impose a more demanding scenario, a step disturbance with an amplitude of approximately 8–10 % of the nominal reference pressure was applied at an appropriate simulation instant. As shown in Fig. 11, the FGO-based 2-DOF PI controller maintains accurate tracking of the reference pressure with minor, short-lived deviations, demonstrating high resilience in noisy and disturbance-prone conditions.

Table 5
Comparisons of normalized time response specifications.

Control mechanism	Rise time (s)	Settling time (s)	Overshoot (%)
FGO-based 2-DOF PI	**0.1172**	**0.2120**	**0**
Rovira-based 2-DOF PID	0.2286	0.3910	0.4066
Cohen-Coon-based PID	0.2913	0.4615	0.8442

To quantitatively evaluate the closed-loop performance under disturbance and noise conditions (Fig. 11), four widely used error-integral performance indices are calculated: IAE, Integral Squared Error (ISE), Integral Time Absolute Error (ITAE) and Integral Time Squared Error (ITSE). These indices provide complementary perspectives on tracking accuracy, transient performance, and the penalization of sustained errors. They are defined as:

$$IAE = \int_0^{t_f} |e(t)|dt \tag{30}$$

$$ISE = \int_0^{t_f} e^2(t)dt \tag{31}$$

$$ITAE = \int_0^{t_f} t|e(t)|dt \tag{32}$$

$$ITSE = \int_0^{t_f} te^2(t)dt \tag{33}$$

where $e(t)$ is the tracking error and $t_f = 20$ s is the total simulation time. The computed values for the proposed FGO-tuned 2-DOF PI controller and the comparative methods (NRBO, L-SHADE, GA) are summarized in Table 6. These results indicate that the proposed controller achieves the lowest IAE, ISE, ITAE, and ITSE values among all methods, confirming its superior capability in reducing both the magnitude and duration of the tracking error under adverse operating conditions.

In addition to the performance metrics reported earlier, we evaluated the computational complexity of the FGO algorithm in comparison with GA, L-SHADE, and NRBO to provide a complete picture of their practical feasibility. All algorithms were executed under identical conditions, using the same number of iterations and population size for a fair assessment. Furthermore, each algorithm employed the default parameter settings recommended in the original literature to ensure unbiased performance comparison while preserving their intended search dynamics.

The average execution time per run for each algorithm was recorded over 25 independent runs. The FGO achieved the shortest execution time, averaging 355.6772 s, followed by L-SHADE (376.5220 s), NRBO (408.5422 s), and GA (653.1078 s). These results indicate that the proposed FGO not only outperforms competing algorithms in terms of control performance but also exhibits competitive computational efficiency.

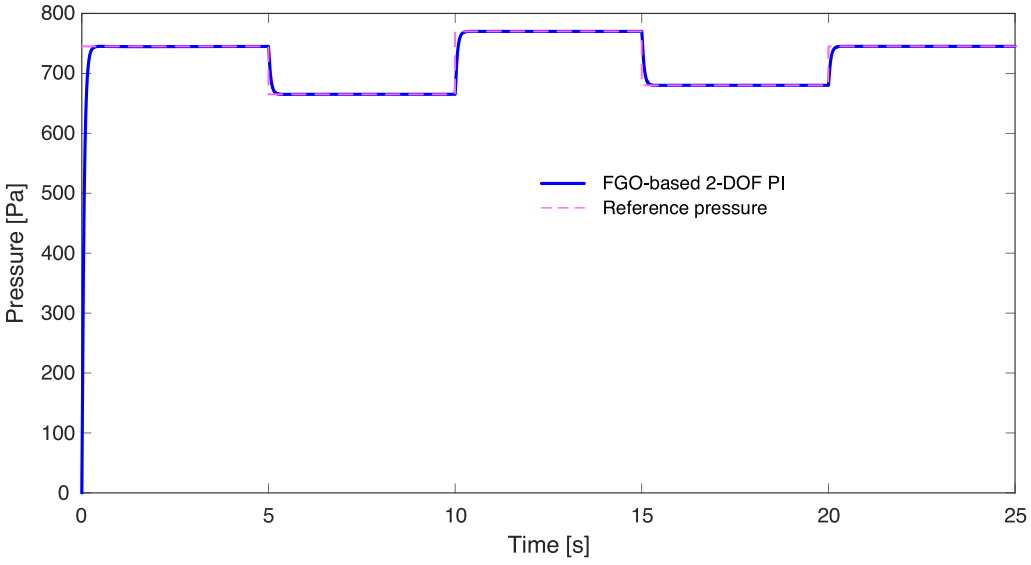


Fig. 9. Pressure tracking performance of proposed FGO-based 2-DOF PI controller.

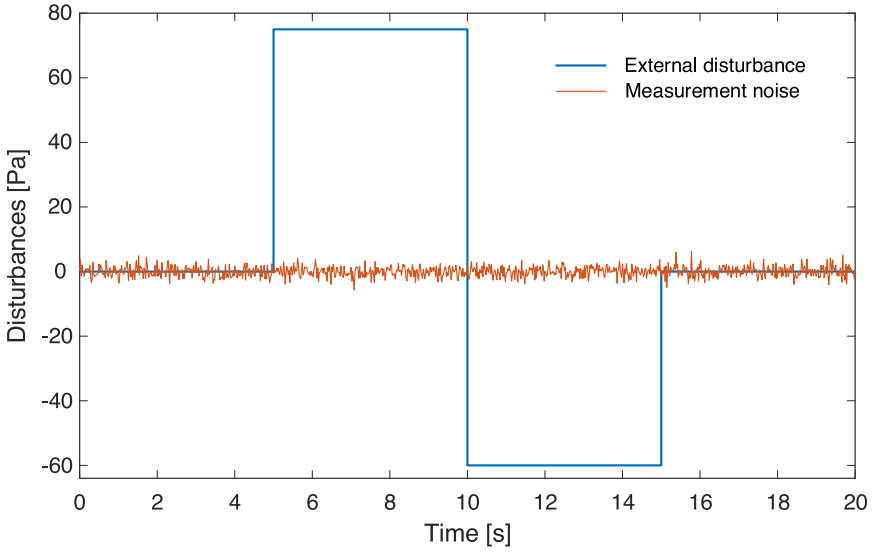


Fig. 10. Profiles of external disturbances and measurement noise injected into the system.

It is important to note that, while the execution times reported here are acceptable for offline controller tuning, the computational cost of metaheuristic algorithms may pose limitations for real-time or online adaptation in fast-changing industrial processes. Nonetheless, the relatively lower execution time of FGO compared to the other metaheuristics suggests that it could be adapted to quasi-online scenarios or periodic re-tuning strategies, especially when combined with model reduction techniques or parallel processing.

6. Conclusion and future work

This paper introduced a novel FGO-tuned two-degree-of-freedom PI controller for pressure control in a centrifugal fan driven by an induction motor. The controller was developed based on an experimentally validated nonlinear dynamical model and optimized using FGO, a recent metaheuristic inspired by the adaptive behavior of fungi. Comparative assessments with classical tuning methods (Cohen-Coon and Rovira) and widely adopted metaheuristics (GA, L-SHADE, and NRBO) revealed that the proposed method offers significant improvements in convergence speed, cost function minimization, and time-domain response characteristics. In particular, the FGO-based controller achieved the shortest rise and settling times while eliminating overshoot and ensuring accurate steady-state tracking. Robustness analyses further confirmed the controller's resilience under piecewise reference variations, external disturbances and noise. The statistical significance of the results was validated via the Wilcoxon signed-rank test, reinforcing the superiority of the proposed approach. The integration of the FGO with a 2-DOF PI framework not only enhances dynamic performance but also maintains

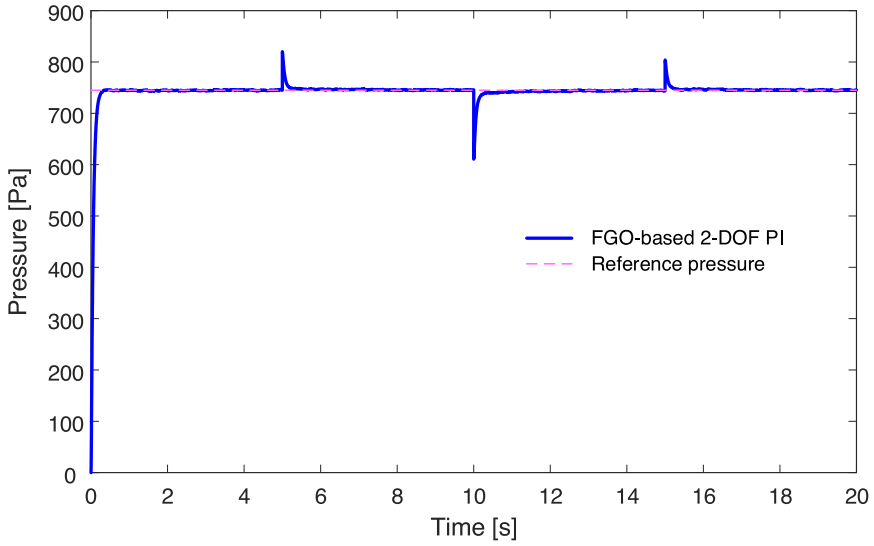


Fig. 11. Pressure response of the FGO-based 2-DOF PI controller under disturbance and noise conditions.

Table 6
Error-integral performance indices for different algorithms.

Algorithm	*IAE* [Pa.s]	*ISE* [Pa^2.s]	*ITAE* [$Pa.s^2$]	*ITSE* [$Pa^2.s^2$]
FGO	**92.3664**	**1.8991E+ 04**	**488.3851**	**1.0491E+ 04**
NRBO	114.8946	2.0676E+ 04	688.2141	1.2681E+ 04
L-SHADE	100.2602	1.9776E+ 04	554.0693	1.1352E+ 04
GA	107.7389	2.2443E+ 04	560.4045	1.2801E+ 04

structural simplicity, making it suitable for real-world implementation in industrial environments.

While the proposed framework delivers high performance and robustness, certain considerations remain. As with most metaheuristics, the performance of FGO can be influenced by parameter selection and its stochastic nature, which may result in varying convergence behaviors across runs. The current study was conducted within a high-fidelity simulation environment; validating the approach through hardware-in-the-loop testing and full-scale industrial experiments would further strengthen its practical credibility. Future work may explore adaptive or hybrid FGO variants for enhanced convergence reliability, extend the tuning methodology to other advanced control architectures, and incorporate multi-objective formulations that balance tracking performance with energy efficiency. These directions have the potential to broaden the applicability of the proposed method to a wider range of turbomachinery and complex process control systems.

CRediT authorship contribution statement

Oleh Kiselychnyk: Writing – review & editing, Supervision, Methodology, Funding acquisition, Conceptualization. **Davut Izci:** Writing – review & editing, Validation, Supervision, Methodology, Formal analysis. **Serdar Ekinci:** Writing – original draft, Validation, Software, Methodology, Formal analysis, Data curation, Conceptualization. **Cebrail Turkeri:** Writing – original draft, Validation, Software, Methodology, Formal analysis, Conceptualization.

Funding

This work in part was conducted within the research project 'Joint UK-India Clean Energy Centre (JUICE)' which was funded by the RCUK's Energy Programme (contract no: EP/P003605/1). The project funder was not directly involved in the writing of this article.

Declaration of Competing Interest

The authors declare the following financial interests/personal relationships which may be considered as potential competing interests: Oleh Kiselychnyk reports financial support was provided by UK Research and Innovation. If there are other authors, they declare that they have no known competing financial interests or personal relationships that could have appeared to influence the work reported in this paper.

References

[1] Ji J, Pan C, Zhang W, Wei Y. Toward non-swirling uniform inflow and stabilized flow in a centrifugal turbomachine model with an intake elbow using rotational guide vanes. Phys Fluids 2025;37:057117. https://doi.org/10.1063/5.0266629.
[2] Ji C, Wang Z, Xi G. Adaptive batch sampling strategy for the hundreds-dimensional aerodynamic optimization of the centrifugal impeller. J Turbomach 2024;146:091003. https://doi.org/10.1115/1.4065050.
[3] Meroni A, Zühlsdorf B, Elmegaard B, Haglind F. Design of centrifugal compressors for heat pump systems. Appl Energy 2018;232:139–56. https://doi.org/10.1016/j.apenergy.2018.09.210.
[4] Liang D, Yang H, Xu C, Jiang Y, Yi Z. The recent progresses in industrial centrifugal compressor designs. Int J Fluid Mech Therm Sci 2020;6:61–9. https://doi.org/10.11648/j.ijfmts.20200602.13.
[5] Came P, Robinson C. Centrifugal compressor design. Proceedings Institution Mechanical Engineers Part C Journal Mechanical Engineering Science 1998;213:139–55. https://doi.org/10.1243/0954406991522239.
[6] Kurz R, Mistry J, Davis P, Cole G. Application and control of variable speed centrifugal compressors in the oil and gas industry. IEEE IAS Pet Chem Ind Tech Conf (PCIC) 2021:273–82. https://doi.org/10.1109/PCIC42579.2021.9729018.
[7] Lu L, Cai W, Xie L, Li S, Soh YC. HVAC system optimization-in-building section. Energy Build 2005;37(1):11–22. https://doi.org/10.1016/j.enbuild.2003.12.007.
[8] Olatunde T, Okwandu A, Akande D, Queen Z. Review of energy-efficient HVAC technologies for sustainable buildings. Int J Sci Technol Res Arch 2024;6(2):12–20. https://doi.org/10.53771/ijstra.2024.6.2.0039.
[9] Turkeri C. Control-oriented dynamical modelling and state estimation of centrifugal fans with induction motor drives (Doctoral dissertation, University of Warwick). Warwick Res Arch Portal 2023. ⟨https://wrap.warwick.ac.uk/185568/1/WRAP_Theses_Turkeri_2023.pdf⟩.
[10] Wang W, Deng Q, Pei J, Chen J, Gan X. Discrete Optimization on Unsteady Pressure Fluctuation of a Centrifugal Pump Using ANN and Modified GA. Chin J Mech Eng 2023;36:84. https://doi.org/10.1186/s10033-023-00915-4.
[11] Blum D, Wang Z, Weyandt C, Kim D, Wetter M, Hong T, Piette MA. Field demonstration and implementation analysis of model predictive control in an office HVAC system. Appl Energy 2022;318:119104. https://doi.org/10.1016/j.apenergy.2022.119104.
[12] Rigatos G, Abbaszadeh M, Sari B, Siano P, Cuccurullo G, Zouari F. Nonlinear optimal control for a gas compressor driven by an induction motor. Results Control Optim 2023;11:100226. https://doi.org/10.1016/j.rico.2023.100226.
[13] Rigatos G, Sari B, Siano P, Abbaszadeh M. Nonlinear optimal control for a gas compressor actuated by a five-phase induction motor. Power Electron Drives 2023;8:196–218. https://doi.org/10.2478/pead-2023-0014.

[14] Morari M, Grammatico S, Cortinovis A, Torrisi G, Smith R, Mercangöz M. Model predictive approaches for active surge control in centrifugal compressors. IEEE Trans Control Syst Technol 2017;25:1947–60. https://doi.org/10.1109/TCST.2016.2636027.
[15] Zhang R, Zhang D, Xu B, Zhao X. A comparative study of Gaussian process regression with other three machine learning approaches in the performance prediction of centrifugal pump. Proceedings Institution Mechanical Engineers Part C Journal Mechanical Engineering Science 2021;236:3938–49. https://doi.org/10.1177/09544062211050542.
[16] Kiselychnyk O, Bodson M. Nonsensor control of centrifugal water pump with asynchronous electric-drive motor based on extended Kalman filter. Russ Electr Eng 2011;82:69–75.
[17] Pechenik M, Kiselychnyk O, Buryan S, Petukhova D. Sensorless control of water supply pump based on neural network estimation. Electrotech Comput Syst 2015;3:462–6.
[18] Turkeri C, Kiselychnyk O. Dynamical modelling of a centrifugal fan driven by an induction motor and experimental validation. Energies 2023;16(18):6658. https://doi.org/10.3390/en16186658.
[19] Devan PAM, Hussin FA, Ibrahim R, Bingi K, Abdulrab H. Design of fractional-order predictive PI controller for real-time pressure process plant. 2021 Aust NZ Control Conf (ANZCC) Gold Coast Aust 2021:86–91. https://doi.org/10.1109/ANZCC53563.2021.9628377.
[20] Pan Y, Wang Y. Fuzzy PI Control and Optimization of Startup Process of High-Speed DC Centrifugal Pumps. Recent Innov Chem Eng 2025;18(2):147–63. https://doi.org/10.2174/0124055204374433250310084724.
[21] Hassan S, Bingi K, Harindran V, Ibrahim R, Karsiti M. Real-Time Control of Pressure Plant Using 2DOF Fractional-Order PID Controller. Arab J Sci Eng 2019;44:2091–102. https://doi.org/10.1007/S13369-018-3317-9.
[22] Coskun M, Itik M. Intelligent PID control of an industrial electro-hydraulic system. ISA Trans 2023;139:484–98. https://doi.org/10.1016/j.isatra.2023.04.005.
[23] Valério D, Costa J. Tuning of fractional PID controllers with Ziegler-Nichols-type rules. Signal Process 2006;86(10):2771–84. https://doi.org/10.1016/j.sigpro.2006.02.020.
[24] Isdaryani F, Feriyonika F, Ferdiansyah R. Comparison of Ziegler-Nichols and Cohen Coon tuning method for magnetic levitation control system. J Phys Conf Ser 2020;1450(1):012033. https://doi.org/10.1088/1742-6596/1450/1/012033.
[25] Rojas JD, Arrieta O, Vilanova R. Industrial PID Control. Industrial PID Controller Tuning. Advances in Industrial Control. *Cham*: Springer; 2021. https://doi.org/10.1007/978-3-030-72311-8_2.
[26] Olaiya OO, Joseph E. Cohen-Coon PID tuning method: a better option to Ziegler Nichols-pid tuning method. Comput Eng Intell Syst 2018;9:33–7. ⟨https://api.semanticscholar.org/CorpusID:55144911⟩.
[27] Paul H, Chatterjee R, Paul S, Sanyal A, Pandey I. An enhanced auto-tuning approach for PID controllers. Am J Adv Comput 2023;2(2):33–7. https://doi.org/10.15864/ajac.22009.
[28] Nassef A, Abdelkareem M, Baroutaji A, Maghrabie H. Review of metaheuristic optimization algorithms for power systems problems. Sustainability 2023;15(12):9434. https://doi.org/10.3390/su15129434.
[29] Belgaid Y, Helaimi M, Taleb R, Youcef M. Optimal tuning of PI controller using genetic algorithm for wind turbine application. Indones J Electr Eng Comput Sci 2020;18:167–78. https://doi.org/10.11591/ijeecs.v18.i1.pp167-178.
[30] Qi H, Li W, Ji L, Liu M, Song R, Pan Y, Yang Y. Performance optimization of centrifugal pump based on particle swarm optimization and entropy generation theory. Front Energy Res 2023;10:1094717. https://doi.org/10.3389/fenrg.2022.1094717.
[31] Amodeo L, Younsi K, Yalaoui F, Tairi A, Chebouba A, Smati A. Optimization of natural gas pipeline transportation using ant colony optimization. Comput Oper Res 2009;36:1916–23. https://doi.org/10.1016/j.cor.2008.06.005.
[32] Tabak A, Ilhan I. An effective method based on simulated annealing for automatic generation control of power systems. Appl Soft Comput 2022;126:109277. https://doi.org/10.1016/j.asoc.2022.109277.
[33] Ekinci S, Turkeri C, Izci D, Abualigah L, Bajaj M, Blazek V, Prokop L. A novel pressure control method for nonlinear shell-and-tube steam condenser system via electric eel foraging optimizer. Sci Rep 2025;15:7550. https://doi.org/10.1038/s41598-025-92576-7.
[34] Nail B, Bekhiti B, Puig V. Internal stability improvement of a natural gas centrifugal compressor system based on a new optimal output feedback controller using block transformation and grey wolf optimizer. J Nat Gas Sci Eng 2020;85:103697. https://doi.org/10.1016/j.jngse.2020.103697.
[35] Rawat T, Ashok A, Singh S. Nonlinear System Identification Using Adaptive Volterra Model Optimized with Sine Cosine Algorithm. Arab J Sci Eng 2022;47:14411–22. https://doi.org/10.1007/s13369-022-06800-x.
[36] Sowmya R, Premkumar M, Jangir P. Newton-Raphson-based optimizer: A new population-based metaheuristic algorithm for continuous optimization problems. Eng Appl Artif Intell 2024;128:107532. https://doi.org/10.1016/j.engappai.2023.107532.
[37] Jin Q, Jiang B, Wang Q, Qi L. Novel improved cuckoo search for PID controller design. Trans Inst Meas Control 2014;37(6):721–31. https://doi.org/10.1177/0142331214544211.
[38] Huang W, Liu D, Li J. Real-time solution of unsteady inverse heat conduction problem based on parameter-adaptive PID with improved whale optimization algorithm. Energies 2022;16(1):225. https://doi.org/10.3390/en16010225.
[39] Tanabe R, Fukunaga AS. Improving the search performance of SHADE using linear population size reduction. Beijing, China: 2014 IEEE Congress on Evolutionary Computation (CEC); 2014. p. 1658–65. https://doi.org/10.1109/CEC.2014.6900380.
[40] Abdel-Basset M, Mohamed R, Abouhawwash M. Fungal growth optimizer: a novel nature-inspired metaheuristic algorithm for stochastic optimization. Comput Methods Appl Mech Eng 2025;437:117825. https://doi.org/10.1016/j.cma.2025.117825.
[41] Haddad AG, Boiko I, Al-Durra A. Oxygen-sensor-based 2-DOF PI air-flow controller of fuel cell system. J Frankl Inst 2024;361(17):107227. https://doi.org/10.1016/j.jfranklin.2024.107227.
[42] Sun L, Li D, Lee KY. Optimal disturbance rejection for PI controller with constraints on relative delay margin. ISA Trans 2016;63:103–11. https://doi.org/10.1016/j.isatra.2016.03.014.